Title: Evaluation of corrosion resistance of nanotubular oxide layers on the Ti13Zr13Nb alloy in physiological saline solution

Author: Agnieszka Smołka, Grzegorz Dercz, Karolina Rodak, Bożena Łosiewcz

Citation style: Smołka Agnieszka, Dercz Grzegorz, Rodak Karolina, Łosiewcz Bożena. (2015). Evaluation of corrosion resistance of nanotubular oxide layers on the Ti13Zr13Nb alloy in physiological saline solution. "Archives of Metallurgy and Materials" (2015, iss. 4, s. 2681-2686), doi 10.1515/amm-2015-0432

A R C H I V E S O F M E T A L L U R G Y A N D M A T E R I A L S
Volume 60 2015 Issue 4
DOI: 10.1515/amm-2015-0432

A. SMOŁKA*#, G. DERCZ*, K. RODAK**, B. ŁOSIEWICZ**

EVALUATION OF CORROSION RESISTANCE OF NANOTUBULAR OXIDE LAYERS ON THE Ti13Zr13Nb ALLOY IN PHYSIOLOGICAL SALINE SOLUTION

OCENA ODPORNOŚCI KOROZYJNEJ NANOTUBULARNYCH STRUKTUR TLENKOWYCH NA STOPIE Ti13Zr13Nb W ŚRODOWISKU PŁYNÓW USTROJOWYCH"

Evaluation of corrosion resistance of the self-organized nanotubular oxide layers on the Ti13Zr13Nb alloy, has been carried out in 0.9% NaCl solution at the temperature of 37ºC. Anodization process of the tested alloy was conducted in a solution of 1M $(NH_4)_2SO_4$ with the addition of 1 wt.% NH_4F. The self-organized nanotubular oxide layers were obtained at the voltage of 20 V for the anodization time of 120 min. Investigations of surface morphology by scanning transmission electron microscopy (STEM) revealed that as a result of the anodization under proposed conditions, the single-walled nanotubes (SWNTs) can be formed of diameters that range from 10 to 32 nm. Corrosion resistance studies of the obtained nanotubular oxide layers and pure Ti13Zr13Nb alloy were carried out using open circuit potential, anodic polarization curves, and electrochemical impedance spectroscopy (EIS) methods. It was found that surface modification by electrochemical formation of the self-organized nanotubular oxide layers increases the corrosion resistance of the Ti13Zr13Nb alloy in comparison with pure alloy.

Keywords: anodization, corrosion resistance, self-organized nanotubes, Ti13Zr13Nb implant alloy

Przeprowadzono badania oceny odporności korozyjnej nanotubularnych struktur tlenkowych na stopie Ti13Zr13Nb w środowisku płynów ustrojowych. Określono wpływ obecności nanotubularnych struktur tlenkowych na zmianę odporności korozyjnej stopu Ti13Zr13Nb. Proces anodowania elektrochemicznego prowadzono w roztworze 1M $(NH_4)_2SO_4$ z 1 % dodatkiem NH_4F. Samoorganizujące się warstwy nanorurek otrzymano przy napięciu 20 V i czasie anodowania 120 min. Badania morfologii powierzchni metodą skaningowej transmisyjnej mikroskopii elektronowej ujawniły, że w wyniku anodowania w zaproponowanych warunkach można otrzymać nanorurki o średnicy mieszczącej się w zakresie od 10 do 32 nm. Badania odporności korozyjnej nanotubularnych warstw tlenkowych oraz czystego stopu Ti13Zr13Nb przeprowadzono w 0,9 % roztworze soli fizjologicznej NaCl w temperaturze 37ºC z wykorzystaniem metody potencjału obwodu otwartego, krzywych polaryzacji anodowej oraz elektrochemicznej spektroskopii impedancji. Wykazano, iż modyfikacja powierzchni za pomocą formowania nanotubularnych struktur tlenkowych zwiększa odporność korozyjną stopu Ti13Zr13Nb w porównaniu do czystego stopu.

1. Introduction

The global growth in the world population age is reflected in the increase in implant surgery performed. Implant having to find the human body must satisfy two main functions, namely, biocompatibility and biofuncionality [1]. Currently, there is a wide range of metallic biomaterials used as implants [1-7]. The titanium and its alloys are the most commonly used implant materials in medicine since the early 60s of the twentieth century [2, 4]. Their popularity is due to good biomechanical properties, high biocompatibility and excellent corrosion resistance in comparison with other metallic biomaterials such as 316L steel and Co-Cr alloys [3, 4]. In order to increase both the biological activity of titanium and its alloys, and the growth of osseous tissue, various modifications of the surface layer have been applied [2, 3, 7]. Electrochemical surface modification of titanium and its alloys is associated with occuring thin (2-5 nm) oxide layer of TiO_2 which is formed spontaneously as a result of exposure of titanium and its alloys on air. The oxide layer with strong barrier properties protects titanium surface against corrosion. One of the recently developed methods is an electrochemical formation of the self-organized nanotubular oxide layers on the surface of titanium and its alloys by anodization. Formation of the nanotubular oxide layers on the surface of titanium biomaterials has a purpose to enhance the osseointegration between a titanium implant surface and a living bone tissue. The element of titanium implant placed in the bone has a surface on which cell

* UNIVERSITY OF SILESIA, INSTITUTE OF MATERIALS SCIENCE, SILESIAN INTERDISCIPLINARY CENTRE FOR EDUCATION AND RESEARCH, 75 PUŁKU PIECHOTY 1A, 41-500 CHORZÓW, POLAND

** SILESIAN UNIVERSITY OF TECHNOLOGY,FACULTY OF MATERIALS ENGINEERING AND METALLURGY, 8 KRASIŃSKIEGO STR., 40-019 KATOWICE, POLAND

Corresponding author: agnieszka.smolka@us.edu.pl

and tissue healing reactions can occur. These reactions may be identical, but not in each case must be. The nanotubular oxide layers may act as micro- or nanosyringes saturated with microbicides or therapeutic agents, and enable their controlled release into the body with a determined rate which is dependent on the geometry of the pores, thus contributing to the reduction of adverse reactions after implantation. The presence of the nanotubes on the implant surface also contributes to growth of the corrosion resistance of the biomaterial in the environment of simulated body fluids (SBFs) what has been reported in the literature [5-7].

The aim of this study was to obtain the self-organized nanotubular oxide structures on the Ti13Zr13Nb implant alloy by anodization method, and to determine their effect on the corrosion resistance of the Ti13Zr13Nb alloy in physiological saline solution (PSS).

2. Material and research methods

The investigated material was the Ti13wt.%Zr13wt.%Nb alloy. The samples with dimensions of 7.0 x 4.0 x 0.8 mm were cut from flat bars, and mechanically polished before anodization using abrasive papers (Buehler, P 600, P 1200 and P 3000, SiC). Then, they were sonicated for 20 min in ultrapure water (Millipore, resistivity of 18.2 MW cm, < 2 ppb total organic carbon).

The anodization process was carried out in a solution of 1 M $(NH_4)_2SO_4$ with 1 wt.% of NH_4F addition (pH=5) for 120 min at a voltage of 20 V. The formation process of the nanotubular oxide structures was carried out by means of a MAG-5N galvanizing aggregate in the two-electrode system consisting of the working electrode which was the tested sample, and the counter electrode in the form of a platinum foil being spaced from the working electrode for a distance of 25 mm.

The corrosion resistance of the obtained nanotubular oxide structures and comparatively the Ti13Zr13Nb alloy before anodization, was determined in PSS of 0.9% NaCl solution at the temperature of 37 ± 2° C using the method of open-circuit potential (OCP), polarization curves and electrochemical impedance spectroscopy (EIS). In order to ensure an inert atmosphere in the electrochemical cell during the measurements, over the electrolyte surface a constant flow of Ar (99.999% purity) was maintained. In the corrosion investigations, a three-electrode electrochemical cell was used. The working electrode was made of the Ti13Zr13Nb alloy before and after anodization. One side of the sample with the geometric surface area of 0.28 cm^2 was exposed to corrosive medium, the other side was insulated with epoxy resin which has not been in the reaction with the electrolyte. The counter electrode was the platinum foil with the geometric surface area of 2 cm^2. All values of the potentials were measured in relation to the saturated calomel electrode (SCE). Electrochemical measurements were carried out using a computer-controlled Metrohm/Eco Chemie Autloab PGSTAT30 Potentiostat/ Galvanostat Electrochemical System. The corrosion tests included the measurements of the open circuit potential, E_{OC}, for 2 h, after which the anodic polarization curves were recorded in the potential range of ± 50 mV versus the stable E_{OC} value at a rate of the electrode polarization of v = 1 mV s^{-1}. The obtained polarization curves were subjected to the Tafel extrapolation in order to determine the following corrosion resistance parameters: corrosion potential, E_{cor}, corrosion current density, j_{cor}, polarization resistance, R_p, cathodic, b_c, and anodic, b_a, Tafel coefficient, respectively, as well as corrosion rate, Cr, at E_{cor} given in mm per year. Calculations were performed according to the standard ASTM G 102-89 [128]. Based on the obtained polarization curves showing the relationship log j = f(E) and using the Tafel extrapolation method, the parameters of the corrosion resistance were determined. The EIS measurements were carried out potentiostatically at a corrosion potential, E_{cor}, determined based on the Tafel extrapolation. Ac impedance spectra were registered in the frequency range of 20 kHz - 1 mHz using 10 frequencies per decade and an excitation signal in the form of a sine wave with an amplitude of 10 mV. The experimental EIS data were analyzed based on the equivalent electrical analogs by means of the EQUIVCRT program [9] and using the non-linear least squares (NLS) method with modulus weighting. The equivalent circuits were defined using circuit description code given by Boukamp [10, 11]. The experimental ac impedance results awere presented as symbols in the form of the Nyquist diagram (also known under the name of a complex plane impedance plot) which is the well-known and generally accepted way of EIS data presentation [12]. It is characterized by the real component of the impedance, Z', on the axis of abscissae, and the imaginary component of the impedance, Z'', on the axis of ordinates. All graphs were created based on the function of Z'' = f (Z'). The experimental impedance spectra for the Ti13Zr13Nb alloy before anodization were approximated using an equivalent electrical circuit (EEC) which slightly differs from the classical Randle's EEC [12]. The obtained results were used for a comparative assessment of the corrosion resistance of the Ti13Zr13Nb before and after anodization.

The morphology of the formed nanotubular oxide layers was examined by scanning transmission electron microscopy (STEM) and scanning electron microscopy (SEM) using a HITACHI HD-2300A and a JEOL JSM-6480 microscope, respectively. The structure was studied by the grazing incidence X-ray diffraction (GIXD) using a X'Pert Philips PW 3040/60 diffractometer operating at 30 mA and 40 kV, which was equipped with a vertical goniometer and an Eulerian cradle. The wavelength of radiation (λCuKα) was 1.54178 Å. The GIXD patterns were registered in the 2θ range from 10 to 50° with a 0.05° step for the incident 0.25°, 0.50°, 1.00° angle.

3. Results and discussion

A STEM microphotograph of the Ti13Zr13Nb alloy surface after anodization process carried out at a potential of 20 V for 120 min in 1M $(NH_4)_2SO_4$ with 1 wt.% of NH_4F addition is shown in Fig. 1. One can observe characteristic cracks and narrow crevices on the alloy surface which are caused by dissolution of the oxide layer formed in the initial phase of oxidation. The obtained barrier layer of the oxides on the alloy surface due to tight adherence to the substrate and low conduction may influence the reduction of the corrosion rate of

the tested biomaterial. In the cracks and crevices, the oxide layer dissolution proceeded, and initially pores and finally the self-organized nanotubular oxide layers, were formed. The detailed mechanism of the multistep formation of the titanium oxide single-walled nanotubes (SWNTs) on the Ti13Zr13Nb alloy as well as their physico-chemical characteristics were shown in our earlier work [13]. The anodization process of the Ti13Zr13Nb alloy under proposed conditions allowed to obtain the TiO_2 SWNTs with an internal diameter in the range from 12 to 32 nm.

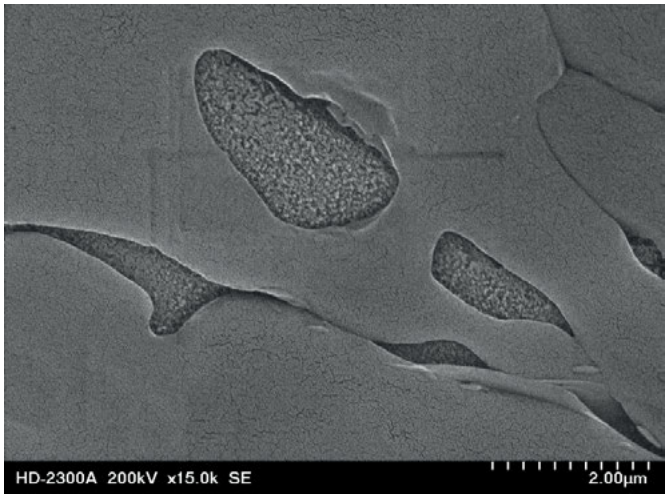

Fig. 1. STEM microphotograph (top view) showing the surface morphology of the Ti13Zr13Nb alloy with the TiO_2 SWNTs produced in the cracks and crevices

The phase analysis of the substrate, Ti13Zr13Nb alloy, showed two phases: α-Ti (ICDD PDF 03-065-3362) and β-Ti (ICDD PDF 01-089-4913). The presence of titanium oxide (TiO_2 rutile, ICDD PDF 00-034-0180) on the surface of the Ti13Zr13Nb alloy after anodization at 20 V for 120 min, was confirmed using the GIXD technique in the previous work [13].

The potentiodynamic curves of log j = f(E) registered in PSS in the narrow range of potentials for the Ti13Zr13Nb alloy before and after anodic oxidation are presented in Fig. 2. The equivalent weight, EW, for the Ti13Zr13Nb alloy of 12.5 was applied. The thermodynamically stable forms of Ti^{4+}, Zr^{2+} and Nb^{5+} under experimental conditions were estimated based on the Pourbaix diagram for Ti-H_2O, Zr-H_2O and Nb-H_2O system, respectively [14]. The alloy density of d = 4.66 gcm^{-3} was used in calculations [15]. Summary of the determined parameters with their standard deviations is presented in Table 1.

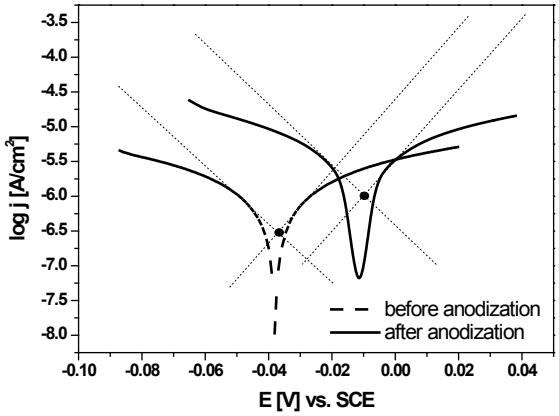

Fig. 2. The potentiodynamic curves of log j = f(E) registered in PSS of 0.9% NaCl at 37°C for the Ti13Zr13Nb alloy before (dashed line) and after (straight line) anodic oxidation

E_{cor} and j_{cor} values were precisely determined at the intersection of the extrapolated Tafel lines for anodic and cathodic branches (Fig. 2). One can see that for the electrode after anodization process, E_{cor} is slightly shifted towards noble potentials and an increase in j_{cor} value is observed as compared with the corresponding parameters determined for the unmodified electrode. Such a character of changes in electrochemical corrosion behavior of the Ti13Zr13Nb electrode is connected with the presence of the nanotubular oxide layer on the electrode surface. The value of E_{cor} = -0.011±0.002 V points that corrosion process will start later on the electrode after anodization. The value of j_{cor} is proportional to the corrosion rate. It can be also supposed that the thicker oxide layer, the higher corrosion current denisty value is registered as in that case of the obtained nanotubular oxide layer. For the Ti13Zr13Nb electrode before anodization, the value of b_c and b_a Tafel coefficient was 0.018±0.004 and 0.012±0.002 V dec^{-1}, respectively, while for the electrode after anodization b_c = 0.017±0.003 V dec^{-1} and b_a = 0.014±0.003 V dec^{-1} (Table 1). Based on the slopes of the Tafel lines shown in Fig. 2 as dotted lines, it can be expected that in both considered cases the rate of cathodic processes will be faster than the reaction of oxidation. The cathodic process proceeding in PSS can be the reduction of hydrogen ions according to the following equation:

TABLE 1
The corrosion resistance parameters determined by the Tafel extrapolation method in PSS of 0.9% NaCl at 37°C for the Ti13Zr13Nb alloy before and after anodic oxidation

Ti13Zr13Nb alloy	E_{cor} [V]	j_{cor} [A cm^{-2}]	R_p [Ω cm^2]	b_c [V dec^{-1}]	b_a [V dec^{-1}]	CR at E_{cor} [mm yr^{-1}]
Before anodization	-0.038 ±0.008	$3.31 \cdot 10^{-7}$ ±$6.62 \cdot 10^{-8}$	460 ±92	0.018 ±0.004	0.012 ±0.002	0.003 ±0.001
After anodization	-0.011 ±0.002	$1.11 \cdot 10^{-6}$ ±$2.22 \cdot 10^{-7}$	145 ±29	0.017 ±0.003	0.014 ±0.003	0.010 ±0.002

$$2H^+ + 2e \rightarrow H_2 \quad (1)$$

The occurring anodic process is the reaction of dissolution of the alloy component. The b_c and b_a Tafel coefficients obtained for the Ti13Zr13Nb electrode before and after anodization have similar values within the calculated error range. The lower value of R_p and the higher corrosion rate at E_{cor} for the anodized electrode can be explained by the presence of porous nanotubular structure. Inside pores on the surface, the corrosion process will proceed faster due to a local change of solution pH, however, the barrier oxide layer tightly adherent to the substrate assures enough corrosion resistance leading to the conclusion that the method of electrochemical formation of the nanotubular oxide structure provides high corrosion resistance for Ti113Zr13Nb biomaterial in PSS. The obtained results confirm that the tested alloy devoid of the TiO_2 SWNTs is characterized by a slightly lower corrosion resistance as compared to the alloy anodized under proposed conditions. This is consistent with the literature data according to which the presence of the nanotubular oxide structures increases the corrosion resistance in SBFs [1-4].

EIS was used to characterize the interfacial properties of the Ti13Zr13Nb | TiO_2 | PSS and Ti13Zr13Nb | TiO_2 SWNTs | PSS system. For this purpose, the EIS spectra were recorded in physiological saline solution at 37°C at the value of E_{cor}.

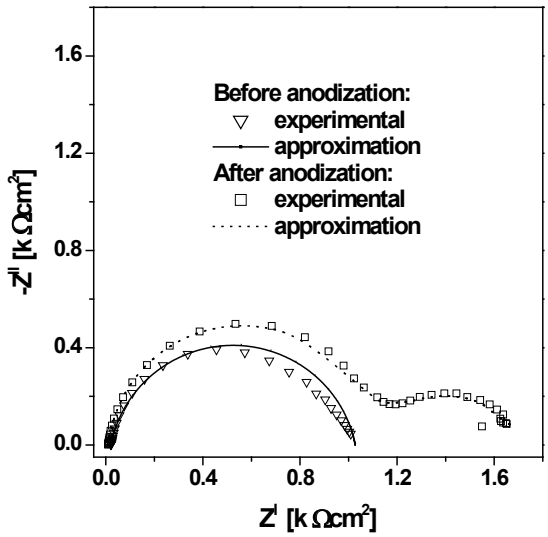

Fig. 3. Nyquist diagram registered at E_{cor} in PSS of 0.9% NaCl at 37°C for the Ti13Zr13Nb alloy before and after anodization

Figure 3 presents impedance spectra obtained at E_{cor} for the Ti13Zr13Nb alloy before and after anodiziation with experimental (symbols) and fitted (lines) data. In case of the unmodified alloy a single semi-circle is observed in the whole range of frequencies studied. Such ac impedance behavior in corrosion process is typical for titanium and its alloys undergoing to natural self-passivation [16]. For the Ti13Zr13Nb alloy with nanotubes formed on its surface in the Nyquist diagram two semi-circles are visible in Fig. 3, wherein the diameter of the first semi-circle registered at high frequencies (HF) is much greater than for the second semi-circle obtained at low frequencies (LF). Such a change in the shape of EIS spectrum in comparison with the impedance spectrum obtained for the Ti13Zr13Nb alloy with thin oxide film on the surface formed as a result of natural self-passivation, may indicate that the impedance response at HF is derived from the outside part of the TiO_2 SWNTs layer (the porous material) being in contact with the electrolyte, and the LF semi-circle obtained at LF is related to the inner barrier TiO_2 film closely adherent to the substrate (which is the essential protection against corrosion of the Ti13Zr13Nb electrode). This impedance behavior is similar to that found for porous Ti electrode covered with nanotubular oxide layer in SBF solution [15].

In this simple CPE model which represents the physical model of the corrosion process of thin oxide layer | PSS system (Fig. 4a), R_s is the solution resistance being in series with a parallel connection of R_{ox}-CPE_{dl} elements. Rox is the resistance of charge transfer through the oxide layer | PSS interface, and the electrical double layer capacitance, C_{dl}, to approximation procedure was substituted by a constant phase element (CPE) [12]. Its impedance is:

$$\hat{Z}_{CPE} = \frac{1}{T(j\omega)^{\phi}} \quad (2)$$

where T (in F cm^{-2} $s^{\phi-1}$) denotes the capacitance parameter, and $\phi \leq 1$ is a dimensionless CPE exponent related to the constant phase angle, $\alpha = 90°(1-\phi)$. The CPE model explains the impedance behavior of a smooth electrode [12] and leads to a rotated single semi-circle on the Nyquist diagram.

The values of C_{dl} for the oxide layer | PSS interface were determined from the formula given by Brug et al. [17]:

$$T = C_{dl}^{\phi}(R_s^{-1} + R_{ct}^{-1})^{1-\phi} \quad (3)$$

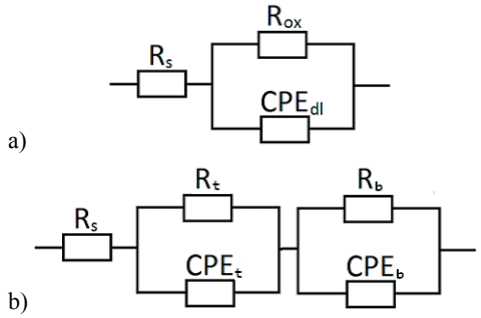

Fig. 4. Equivalent circuit model used for approximation of the experimental EIS data for the system: a) Ti13Zr13Nb | TiO_2 | PSS, and b) Ti13Zr13Nb | TiO_2 SWNTs | PSS at 37°C

The impedance spectra obtained for the Ti13Zr13Nb alloy with nanotubular oxide layers were interpreted using the model containing two CPEs instead of capacitors (Fig. 4b). This EEC consists of the solution resistance in series with two parallel CPE-R elements, where R_t is resistance of the outer tube layer, CPE_t represent the capacitance of the outer tube layer, R_b is resistance of the inner-barrier layer, and CPE_b

denotes capacitance of the inner-barrier layer [5]. This model explains the impedance behavior of an porous electrode, and produces two semi-circles on the Nyquist diagram where the HF semi-circle is related to the surface porosity (nanotubular oxide structure), and the LF semi-circle is related to the charge-transfer process through the inner-barrier oxide layer | PSS interface.

All registered impedance plots were analysed using the NLS method. The best fit to the experimental data for the Ti13Zr13Nb | TiO_2 | PSS and Ti13Zr13Nb | TiO_2 SWNTs | PSS system was obtained using the CPE and two-CPE model, respectively. The approximations of the Nyquist plots (Fig. 3) using the appropriate models from Figs. 4a and b, were very good. The Bode diagrams displayed in Figs. 5 and 6 also confirm good quality of approximations. The results of approximations with their standard deviations are shown in Tables 2 and 3.

In case of the smooth Ti13Zr13Nb electrode before anodization, the R_s parameter has a higher value of 20.69±0.02 Ω cm^2 (Table 2) as compared with R_s = 9.41±0.09 Ω cm^2 determined for the porous electrode after TiO_2 SWNTs anodic formation (Table 3).

The value of charge transfer resistance through the Ti13Zr13Nb | TiO_2 | PSS interface is R_{ox} = 1.01±0.01 kΩ cm^2 (Table 2). This value is slightly lower than R_t = 1.03±0.01 kΩ cm^2 and significantly higher than R_b = 707±18 Ω cm^2 (Table 3) obtained for the Ti13Zr13Nb | TiO_2 SWNTs | PSS interface. It means that the kinetics of electrochemical corrosion in PSS is a little bit slower on the anodized Ti13Zr13Nb electrode as compared with that biomaterial devoid of the presence of TiO_2 SWNTs. Moreover, these data are in good agreement with the results of the Tafel analysis (Table 1), and the literature reports on the corrosion resistance of the self-organized nanotubular oxide layers on titanium and its alloys in SBFs [14].

It should be added that for the anodized Ti13Zr13Nb electrode higher values of parametres characterizing the CPE elements (CPE-T_t and corresponding CPE-ϕ_t, CPE-T_b and corresponding CPE-ϕ_b) were obtained (Table 3) than in case of the same type of electrode but before anodization (CPE-T_{dl} and corresponding CPE-ϕ_{dl}) (Table 2). In Table 3, the higher capacitance of the electrical double-layer for the Ti13Zr13Nb electrode with the TiO_2 SWNTs on the surface (C_{dl} = 131±26 μF cm^{-2}) is presented as compared with C_{dl} = 2.13±0.43 μF cm^{-2} calculated according to Eqn. 3 for the unmodified electrode (Table 2). Such a difference in the value of C_{dl} is probably connected with the stronger surface development of the TiO_2 SWNTs layer (the porous material) than in case of the self-passivated thin oxide layer, and it should not be related to the increase in conductivity of the TiO_2 nanotubes.

The Bode diagrams in the form of log |Z| = f (log f) shown in Fig. 5 confirm the increase in the corrosion resistance of the Ti13Zr13Nb alloy after anodization. The increase in the value of log |Z| determined at the lowest frequency studied of f = 1 mHz, is observed for the Ti13Zr13Nb electrode after the applied electro-oxidation. For both types of the studied electrodes, a linear variation between log |Z| and log f with a slope close to –1 in the range of intermediate frequencies is visible what confirms their capacitive behavior.

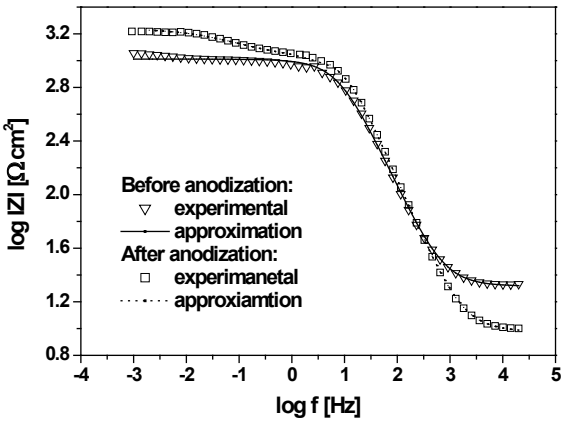

Fig. 5. Comparison of Bode diagrams in the form of log |Z| = f (log f) for the Ti13Zr13Nb alloy before and after the anodization, registered at E_{cor} in PSS of 0.9% NaCl at 37°C

The phase-angle Bode diagrams for the Ti13Zr13Nb alloy before and after anodization are shown in Figure 6. For the self-passivated Ti13Zr13Nb alloy only one time constant is

TABLE 2

Summary of the parameters obtained using the CPE model shown in Fig. 4a to approximate the experimental EIS data for the Ti13Zr13Nb alloy before anodization in 0.9 % NaCl solution at 37°C

Ti13Zr13Nb alloy	R_s [Ω cm^2]	R_{ox} [kΩ cm^2]	CPE-T_{dl} [F cm^{-2} $s^{\phi-1}$]	CPE-ϕ_{dl}	C_{dl} [μF cm^{-2}]
Before anodization	20.69 ±0.02	1.01 ±0.01	$0.73 \cdot 10^{-5}$ $\pm(0.05) \cdot 10^{-5}$	0.877 ±0.008	2.13 ±0.43

TABLE 3

Summary of the parameters obtained using the two-CPE model shown in Fig. 4b to approximate the experimental EIS data for the Ti13Zr13Nb alloy after anodization in 0.9 % NaCl solution at 37°C.

Ti13Zr13Nb alloy	R_s [Ω cm2]	R_t [kΩ cm2]	CPE-T_t [F cm-2 $s^{\phi-1}$]	CPE-ϕ_t	R_b [Ω cm^2]	CPE-T_b [F cm^{-2} $s^{\phi-1}$]	CPE-ϕ_b	C_{dl} [μF cm^{-2}]
After anodization	9.41 ±0.09	1.03 ±0.01	$1.87 \cdot 10^{-5}$ $\pm(3.85) \cdot 10^{-7}$	0.945 ±0.004	707 ±18	0.0020 ±0.0001	0.594 ±0.012	131 ±26

present in the circuit. This is a typical impedance spectrum for the oxide layer on a titanium substrate [15]. One time constant in the circuit can suggest that the corrosion process proceeds by one step via anodic dissolution.

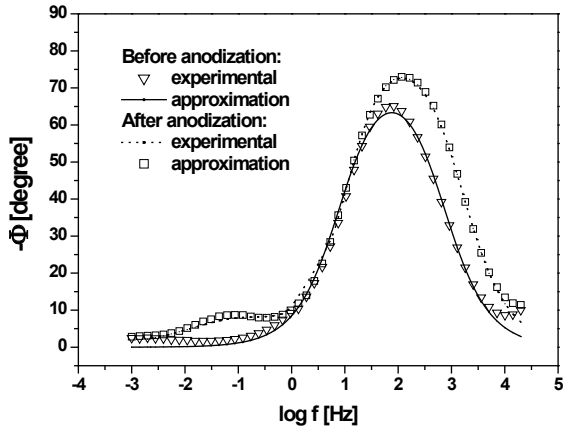

Fig. 6. Phase-angle Bode diagrams for the Ti13Zr13Nb alloy before and after anodic oxidation registered at E_{cor} in PSS of 0.9% NaCl at 37°C

The appearance of the second time constant in the circuit in Fig. 6 for the alloy after anodization indicates the porous surface. The higher values of phase angles close to -90° are observed for the electrode with the TiO_2 SWNTs on the surface. They are typical of a capacitive behavior corresponding to the material covered with the oxide layer with a high corrosion resistance, even in a chloride-containing solutions being well-known to cause pitting.

4. Conclusions

On the basis of the carried out studies by SEM, STEM, and GIXD it was found that surface modification of the Ti13Zr13Nb implant alloy using anodic oxidation allows to obtain the nanotubular oxide structures having an inner diameter of single-wall nanotubes from 10 to 32 nm. EIS studies of the modified alloy showed the typical behavior of impedance for titanium coated with porous oxide layer. Surface modification of the Ti13Zr13Nb alloy increases its corrosion resistance in a physiological saline solution as compared to the alloy surface covered with the self-passivated oxide film. The obtained results suggest that the proposed method of surface modification by anodization is promising for better osseointegration of the Ti13Zr13Nb implants.

Received: 15 September 2015.

Acknowledges

The author received a grant for the project DoktoRIS - Scholarship program for innovative Silesia co-financed by the European Union under the European Social Fund

REFERENCES

[1] S. John Mary, S. Rajendran, Zastita Materijala **53**, 109-113, (2012).
[2] S. Grigorescu, C. Ungureanu, R. Kirchgeorg, P. Schmuki, I. Demetrescu, Appl. Surf. Sci. **270**, 190-196, (2013).
[3] S. Sobieszczyk, Adv. Mater. Sci. **9**, 25-41, (2009).
[4] A.W. Tan, B. Pingguan-Murphy, R. Ahmad, S.A. Akbar, Ceram. Int. **38**, 4421-4435, (2012).
[5] W. Yu, J. Qiu, R. Ahmad, L. Xu, Biomed. Mater. **4**, 1-6, (2009).
[6] V.S. Saji, H.C. Choe, Corros. Sc. **51**, 1658-1663, (2009).
[7] S. Minagar, C. Berndt, J. Wang, E. Ivanova, C. Wen, Acta Biomater. **8**, 2875-2888, (2012).
[8] ASTM G 102-89 (2004). Standard Practice for Calculation of Corrosion Rates and Related Information from Electrochemical Measurements.
[9] User manual for frequency response analysis (FRA) for Windows version 4.9, Eco Chemie B.V., Kanaalweg, Utrecht, The Netherlands, 2001.
[10] B.A. Boukamp, Solid State Ionics **20**, 31-44, (1986).
[11] B.A. Boukamp, Solid State Ionics **18-19**, 136-140, (1986).
[12] A. Lasia, Electrochemical impedance spectroscopy and its applications, in: Modern aspects of electrochemistry, Vol.32, (Eds: B.E. Conway, J. Bockris, and E.E. White), Kluwer Academic/Plenum Publishers, New York, 1999.
[13] A. Smołka, K. Rodak, G. Dercz, W. Simka, K. Dudek, B. Łosiewicz, Acta Phys. Pol., A **125**, 4, 932-935 (2014).
[14] Atlas of Eh-pH diagrams, Intercomparison of thermodynamic databases, National Institute of Advanced Industrial Science and Technology, Naoto TAKENO, 2005.
[15] W-q. Yu, J. Qiu, F-q. Zhang, Colloids Surf. B **84**, 400-405, (2011).
[16] G.J. Brug, A.L.G. van den Eeden, M. Sluyters-Rehabach, J.H. Sluyters, J. Electroanal. Chem. **176**, 275-295, (1984).
[17] L.T. Duarte, S.R. Biaggio, R.C. Rocha-Filho, N. Bocchi, Corros. Sci. **72**, 35-40, (2013).